HHS Public Access

Author manuscript

Nat Biomed Eng. Author manuscript; available in PMC 2019 October 08.

Published in final edited form as:

Nat Biomed Eng. 2019 July ; 3(7): 571–582. doi:10.1038/s41551-019-0381-8.

Comparison of three congruent patient-specific cell types for the modelling of a human genetic Schwann-cell disorder

Bipasha Mukherjee-Clavin[1,2], **Ruifa Mi**[2,3], **Barbara Kern**[4,5], **In Young Choi**[1], **Hotae Lim**[1], **Yohan Oh**[1,&], **Benjamin Lannon**[6,§], **Kevin J. Kim**[7], **Shaughn Bell**[7], **Junho K. Hur**[9], **Woochang Hwang**[11], **Young Hyun Che**[10], **Omer Habib**[9], **Robert H. Baloh**[7,8], **Kevin Eggan**[6], **Gerald Brandacher**[4], **Ahmet Hoke**[2,3], **Lorenz Studer**[12], **Yong Jun Kim**[9,10,*], and **Gabsang Lee**[1,2,3,*]

[1]The Institute for Cell Engineering, Johns Hopkins University School of Medicine, Baltimore, MD 21205, USA

[2]The Solomon H. Snyder Department of Neuroscience, Johns Hopkins University School of Medicine, Baltimore, MD 21205, USA

[3]The Department of Neurology, Johns Hopkins University School of Medicine, Baltimore, MD 21205, USA

[4]The Department of Plastic and Reconstructive Surgery, Vascularized Composite Allotransplantation (VCA) Laboratory, Johns Hopkins University School of Medicine, Baltimore, MD 21205, USA

[5]Department of Surgery, Charité - Universitätsmedizin, Berlin 13353, Germany

[6]Department of Stem Cell and Regenerative Biology, Harvard Stem Cell Institute, Harvard University, Cambridge, MA 02138, USA

[7]Board of Governors Regenerative Medicine Institute, Los Angeles, CA 90048, USA

*Correspondence and requests for materials should be addressed to Y.J.K. or G.L. yjkim1@khu.ac.kr; glee48@jhmi.edu.
&Present address: Department of Medicine, College of Medicine, Hanyang University, Seoul 04763, Korea
§Present address: Boston IVF, Waltham, MA 02451, USA; Department of Obstetrics and Gynecology, Beth Israel Deaconess Medical Center, Boston, MA 02215, USA

Author contributions

B.M-C. and YJ.K.: study design, performing experiments, data analysis, assembly, interpretation, and writing manuscript; R.M., B. K., IY.C., H.L., Y.O., B.L., K.K., S.B., J.K.H., W.H., O.H. and YH.C.: performing experiments and data analysis; K.E.: study design; R.H.B., G.B. and A.H.: conception and study design; L.S.: conception, study design and data analysis; G.L.: conception, performing experiments, data analysis, assembly, interpretation, and writing manuscript.

Reporting summary.

Further information on research design is available in the Nature Research Reporting Summary linked to this article.

Data availability

The authors declare that all data supporting the results in this study are available within the paper and its Supplementary Information. RNA sequencing data from CMT1A and control hESC-SCPs, hiPSC-SCPs, and hiNC-Schwann cells has been uploaded to GEO under accession code GSE85598.

Competing interests

The authors declare no competing interests.

Additional information

Supplementary information is available for this paper at https://doi.org/10.1038/s41551-01X-XXXX-X.

Publisher's note: Springer Nature remains neutral with regard to jurisdictional claims in published maps and institutional affiliations.

[8]Department of Neurology, Cedars-Sinai Medical Center, Los Angeles, CA 90048, USA

[9]Department of Pathology, College of Medicine, Kyung Hee University, Seoul 02447, Korea

[10]Department of Biomedical Science, Graduate school, Kyung Hee University, Seoul 02447, Korea

[11]Data Science for Knowledge Creation Research Center, Seoul National University, Seoul 08826, Korea

[12]Developmental Biology Program, Sloan-Kettering Institute for Cancer Research, New York, NY 10065, USA

Abstract

Patient-specific human induced pluripotent stem cells (hiPSCs) hold great promise for the modelling of genetic disorders. However, these cells display wide intra-individual and inter-individual variations in gene expression, making it challenging to distinguish true-positive and false-positive phenotypes. Also, data from hiPSC phenotypes and from human embryonic stem cells (hESCs) harbouring the same disease mutation are lacking. Here, we report a comparison of molecular, cellular and functional characteristics of three congruent patient-specific cell types — hiPSCs, hESCs, and direct lineage-converted cells — derived from currently available differentiation and direct-reprogramming technologies, for the modelling of Charcot Marie Tooth 1A, a human genetic Schwann-cell disorder featuring a 1.4 megabase chromosomal duplication. In particular, we find that the chemokines CXCL1 and MCP1 are commonly upregulated in all three congruent models and in clinical patient samples. The development of congruent models of a single genetic disease by using somatic cells from a common patient will facilitate the search for convergent phenotypes.

Disease modelling by employing stem cell technologies including human induced pluripotent stem cells (iPSCs) give rise to precise analysis of human diseases which harbor inherited genetic mutations as a causative factor, particularly those in which animal models of molecular and cellular pathophysiology are not fully established[1]. Previous studies using patient somatic cell-derived hiPSCs have recapitulated disease symptom-relevant cell types with individual genetic characteristics and have identified new pathologic mechanism in a cellular level *in vitro*[2]. hiPSC-derived cells are often considered as a developmentally early stage while most human diseases, even genetic ones, are progressive through years to decades. This property of hiPSC-derived cells often limits modelling of neurological disorders while it leads appropriate modelling for congenital abnormalities. Direct reprogramming has been suggested as an alternative to hiPSCs to better model matured cellular phenotypes with aging signatures of converted cells by circumventing the pluripotent state[3]. In that vein, it can be considered a tool for the modelling of late onset diseases since directly converted cells exhibited comparably aged cellular features relative to hiPSCs. In spite of advanced cell fate manipulation tools, however, it is still challenging to accurately model chronic diseases utilizing a single methodology since each are limited by methodology-dependent stage specific cellular charactersistics.

Charcot Marie Tooth 1A (CMT1A) is caused by duplication of a 1.4-mega-base-pairs (Mbp) region on chromosome 17p. It is a hereditary peripheral neuropathy in which Schwann cell pathology results in dysmyelination and demyelination of the peripheral nerves [4,5]. Developing hiPSC models of CMT1A is critical as it is the most common hereditary peripheral neuropathy and currently has no targeted treatments. Furthermore, while rodent models recapitulate many clinical features of CMT1A, they have thus far been limited in their ability to predict therapeutic efficacy of pharmacological treatments. Markedly, ascorbic acid proved robustly effective in treating CMT1A in rodent models[6] yet had much more muted effects in CMT1A clinical trials[7–11].

Here we report the development of a protocol for direct derivation and prospective isolation of Schwann cells from human pluripotent stem cells, use of CMT1A patient hiPSC-derived Schwann cells to model CMT1A pathogenesis, as well as independent validation of those results with CMT1A Schwann cells from PGD-hESCs (Preimplantation Genetic Diagnosis-human embryonic stem cells), and hiNC (human induced Neural Crest). Together, we identified shared molecular and cellular features as a pathologic mechanism of CMT1A from comparing three different methodology-derived congruent Schwann cell models, suggesting integrative analysis of various cell engineering tools as an advanced strategy in disease modelling studies.

Results

Direct differentiation and prospective isolation of Schwann cells from hESCs.

We have devised multiple reprogramming methods for generation of Schwann cell lineage populations and utilized them to model Charcot Marie Tooth 1A, a genetic Schwann cell disorder featuring a 1.4MB chromosomal duplication. We initially created a defined protocol for the direct derivation and prospective isolation of putative Schwann cell precursors (SCPs) from SOX10 reporting human pluripotent stem cells (Fig. 1a-b). The protocol features a 21 day differentiation course and allows for isolation of putative SCPs through alpha 4 integrin CD49d expression (Fig. 1c-d). The purified population features differential global gene expression profiles against hESCs and neural crest, expresses peripheral glia specific genes, and exhibits gliogenesis related gene ontology results (Fig. 1e-f, Table 1). After replating of isolated CD49d+ cells, our protocol permits *in vitro* culture up to 80 days with abundant expression of Schwann cell lineage proteins (Supplementary Fig. 1a). Additionally, when resulting Schwann cell precursors are cultured beyond 35 days, there is a transition in the *PMP22* splice variant expressed (Supplementary Fig. 1b-c) suggesting developmental maturation after prolonged culture[12]. These cells are functional *in vitro* as evidenced by their segmental expression of myelin basic protein when co-cultured with hiPSC-derived TUJ1+ neurons and integrate *in vivo* when transplanted into the murine tibial nerve (Supplementary Fig. 1d-e). Furthermore, in rat models of chronic peripheral nerve denervation that causes a contractured hindpaw,[13,14] injecting hiPSC-derived CD49d+ putative SCPs into the neurorrhaphy site during corrective surgery resulted in a less contractured limb relative to sham treatment. Catwalk gait analysis reveals improved animal standing time, maximum paw contact area, and paw print length and width, demonstrating

that transplanting hiPSC-SCPs can improve functional neuro regeneration *in vivo* as well (Supplementary Fig. 1f).

Modeling CMT1A with patient iPSC-derived Schwann cells.

Next, human induced pluripotent stem cells were created from skin fibroblasts of four CMT1A patients (two parent-child pairs: 5146 & 5148, and 5165 & 5167) and healthy controls, and differentiated into SCPs (Fig. 2a and Supplementary Fig. 2a-c). Upon differentiation, no significant differences were found in SCP yields (Fig. 2b) or Schwann cell marker gene enrichment (Fig. 2c), and real time PCR for *PMP22*, the causal gene in CMT1A, indeed revealed upregulation in the CMT1A hiPSC-SCPs (Fig. 2d). The observed *in vitro* variability in *PMP22* gene expression is in line with clinical observations as well[15]. To find global gene expression differences between CMT1A hiPSC-SCPs and controls, four independently differentiated samples from CMT1A hiPSCs (three samples from one clone from patient 5148, one sample from one hiPSC clone from unrelated patient 5165; samples from remaining CMT1A patients were used for subsequent validation of microarray findings) and controls were submitted for microarray analysis. There is a global pattern of upregulated gene expression in the CMT1A hiPSC-SCPs relative to controls, and notably *PMP22* and *HS3ST3B1*, both genes from the CMT1A duplicated region, are upregulated in the CMT1A hiPSC-SCPs (Fig. 2e). To better understand the broader patterns characterizing the differentially expressed genes, all genes differentially expressed at least 3 standard deviations from the mean were analyzed with Ingenuity Pathway Analysis (IPA; Canonical Pathways function) and DAVID (Biological Process, Cellular Components, and Biocarta functions). Gene ontology analysis reveals that multiple genes in inflammatory signaling pathways (Supplementary Table 1), among unrelated pathways such as extracellular matrix production, were differentially expressed in CMT1A hiPSC-SCPs versus controls. Genes involved in inflammatory responses, the complement system, humoral immunity, granulocyte and agranulocyte adhesion and diapedesis all received statistically significant scores (Fig. 2f). To validate the microarray results, several genes were selected (Fig. 2e, marked genes) and evaluated with qRT-PCR on biologically independent samples from additional CMT1A hiPSC clones and genotypes (Fig. 2g). This implores the question of whether the upregulated inflammatory gene expression translates into increased inflammatory protein expression. Cytokine array analysis of CMT1A and control hiPSC-SCP secretomes demonstrated that CMT1A hiPSC-SCPs secrete greater amounts of 14 (out of 36) proinflammatory proteins profiled (Fig. 2h). Pro-inflammatory cytokines have multiple functions in different contexts, and a common function among those upregulated in the CMT1A hiPSC-SCPs are the ability to recruit monocytes/macrophages or neutrophils to areas of tissue damage.[16,17] A key question in CMT1A research is the role of the *PMP22* gene duplication and increased PMP22 protein expression in CMT1A pathogenesis. Intriguingly, we noticed that extended culture of CMT1A hiPSC-Schwann cells for 35 days further increased PMP22 protein expression (Supplementary Fig. 3a-c), and this correlated with increased inflammatory gene transcription, particularly *MCP1* and *CXCL1*. This raises the question as to whether there may be a correlation between PMP22 expression, inflammatory cytokine upregulation, and CMT1A pathogenesis, and we continue to explore these ideas using additional cellular models of CMT1A.

Establishment of congruent disease models with different methodology-derived CMT1A Schwann cells.

To validate and build upon the observations made in CMT1A hiPSC-SCPs, two complementary models of CMT1A Schwann cells were subsequently employed (Supplementary Table 2): CMT1A PGD-hESCs (human embryonic stem cells isolated from two embryos with a Preimplantation Genetic Diagnosis of CMT1A) (Fig. 3a, Supplementary Fig. 4a-c) and CMT1A hiNC (CMT1A patient fibroblasts directly reprogrammed into Schwann cell lineage via a neural crest intermediate) (Fig 3e). CMT1A PGD-hESCs and healthy controls were differentiated into CD49d+ SCPs using the same methods used for CMT1A hiPSCs (Fig. 3b-d). Next, we utilized a direct conversion technology with the same CMT1A and healthy control patient fibroblasts that were used for hiPSC generation and disease modeling. A single transcription factor, SOX10, was used in combination with WNT activation to convert human fibroblasts into induced neural crest and subsequently Schwann cells[18] (hiNC-SC). Since we observed inflammatory signatures in CMT1A-iPSC-SCPs, we confirmed that hiNC-SCs are indeed Schwann cell lineage with glial marker expression, and not for astrocytes, which is responsible for inflammation in central nervous system (Supplementary Fig. 5a-b). hiNC-SCs were generated from fibroblasts of three CMT1A patients, two of which were included in our earlier hiPSC study. After differentiation of CMT1A and control hiNC towards the Schwann cells (Fig. 3e-f), CMT1A hiNC-Schwann cells demonstrate increased *PMP22* gene expression (Fig. 3g), and the resulting cells from CMT1A and control hiNC exhibit morphological characteristics stereotypical of Schwann cells and immunoreactivity for Schwann cell lineage markers S100B and GFAP (Fig. 3h) with Peripheral glia related gene ontology results from transcriptome profiling (Supplementary Fig. 5c-d).

Next, we analyzed RNA sequencing on 21 samples across our three congruent CMT1A and control Schwann cell models in search of disease relevant phenotypes as well as global differences between hiPSC-, hESC-, and hiNC-derived Schwann cell lineage cells. Remarkably, direct reprogrammed Schwann cells (hiNC-SC) show enrichment of aging related genes and features of DNA damage compared to differentiated Schwann cells (hiPSC-SC) (Supplementary Fig. 6a-b) suggesting that hiNC-derived Schwann cells may represent a more matured or aged state than differentiated SCPs. To validate different features of each Schwann cell population, we compared transcriptome profiles of hiPSC-SCs and hiNC-SCs from healthy control and CMT1A patients. Remarkably, Schwann cell lines were clustered by methodology even when they are differentiated or converted from identical patient fibroblasts (Supplementary Fig. 7a). Furthermore, in conventional gene ontology analysis each model exhibits distinct genetic signatures reflecting their disparate epigenetic origins. Genes involved in early development are upregulated in the hESC-Schwann cell model, features of early development and glial/neuronal commitment are present in the hiPSC-Schwann cell model, and markers of aging, cellular stress, and inflammation are enhanced in the hiNC-Schwann cell model (Supplementary Table 3). Additionally, ontology with analysis with differentially expressed transcriptome between hiPSC-SCs and hiNC-SCs indicates enrichment of compact myelin and anatomic structures in directly converted Schwann cells (Supplementary Fig. 7b), and compact myelination-related genes are upregulated in hiNC-SCs while genes related to myelin sheath formation

are upregulated in identical patient-derived hiPSC-SCs (Supplementary Fig. 7c). Subsequent analysis with CMT1A hiNC-SCs and hiPSC-SCs versus healthy controls reveals that six groups of ontologies (Cell proliferation, Multi-organismal process, Behavior, Response to stimulus, Metabolic process and Presynaptic process involved in chemical synaptic transmission) were inversely expressed in CMT1A vs healthy samples. For example, all genes categorized in plasma lipoprotein particle clearance were reversely expressed in healthy and CMT1A-SCs (Supplementary Fig. 7d-e), which is interesting given that a clinical manifestation of CMT1A is blebbing and rupture of plasma membrane of Schwann cells and formation of lipid droplets inside of nerve tissues due to metabolic dysfunction of Schwann cells.

Signs of DNA damage in directly reprogrammed cells were validated in Supplementary Fig. 6b, and even when the same starting fibroblast is used to make Schwann cells via hiPSC differentiation versus direct reprogramming, only the directly reprogrammed cells have increased γH2AX. γH2AX helps remodel chromatin and repair double-stranded DNA breaks; it is phosphorylated by ATM/ATR which also activates cell cycle check point kinases CHK1/CHK2 to initiate DNA repair. However, none of our cells derived by either method showed any ATM activity, despite directly reprogrammed cells having high levels of γH2AX (Supplementary Fig. 8a-c). Suprisingly, the phosphorylated form of CHK1 and CHK2, were strongly detected in healthy control lines but not CMT1A lines, only when using the differentiation method but not the reprogramming method (Supplementary Fig. 8c). At this time, it is unclear what the underlying mechanism of these DNA-damage related observations are, but to us they represent a feature of direct lineage converted cells that may skew their phenotype, underscoring the importance of using multiple methodologies to minimize biased results from flaws inherent to each single methodology. In light of the multiple clones and individuals in our RNA sequencing data set, we next used a recently developed POWER KIT[19] to further analyze our data. Gene ontology analysis with this second approach showed much distinct separation between models: themes of development/morphogenesis emerged in the hESC model, nervous system development in the hiPSC model, and response to stimuli and cellular adhesion/migration in the hiNC model (Supplementary Table 4). Interestingly, we observed WNT and Notch signaling related ontology in only the hiPSC model, while SMAD signaling related ontologies appeared only in hiNC model which is consistent with prior observations that WNT and Notch are important signaling pathways for early gliogenesis and SMAD signaling functions in de-differentiation, proliferation and death of matured Schwann cells, respectively[20–23]

Immune cell recruitment as a shared pathologic phenotype of CMT1A in congruent models.

To elicit candidate pathologic pathways in CMT1A, we further analyzed transcriptome changes between the three CMT1A-Schwann cell models and controls using both DAVID and Ingenuity Pathway Analysis (Supplementary Tables 5 and 6). Intriguingly, the differentiation-based hESC and hiPSC models showed pathology in developmental signaling pathways and cell cycle related signaling, whereas the direct reprogramming based hiNC model was quite distinct and suggested changes in endocytic trafficking which have been currently proposed in CMT1A research[24] (Fig. 8a and Supplementary Table 6). Despite

these findings, we could not detect any differences in efficiency of Schwann cell precursor generation between CMT1A and controls (Fig. 2b, 3b and 3f). Commonly misregulated pathways amongst all three models include NRF2 signaling, GnRH signaling, retinoic acid signaling and many others which play roles in inflammatory signaling, Schwann cell function, and neuronal function, at least in part via NFKB signaling, a master regulator of both inflammation and myelination[25–28] (Supplementary Fig. 8a and Supplementary Table 6).

To further investigate these inflammatory transcriptional changes, we profiled secreted proteins from independent genotypes of CMT1A and control hESC- and hiNC-Schwann cell models (Supplementary Fig. 9a-d), as had previously been done with hiPSCs (Fig. 2g-h), and we again found statistically significant upregulation of several pro-inflammatory proteins in CMT1A-PGD-hESC- and CMT1A hiNC-Schwann cell models (Supplementary Table 7). By comparing across the CMT1A and control hiPSC, PGD-hESC, and hiNC systems, ultimately two proteins, CXCL1 and MCP1, were found to be commonly upregulated among all three congruent models, resulting in a converged phenotype (Fig. 4a). CXCL1 has been shown to mediate both neutrophil[29] and more recently monocyte[30] chemotaxis in various contexts, and has never been previously implicated in CMT1A pathogenesis. MCP1, also known as macrophage chemoattractant protein-1, is one of the best studied chemokines and is known to robustly induce monocyte migration in a concentration dependent manner.[31] MCP-1 expression has also been reported as upregulated in a rodent model of CMT1A, lending support to our findings.[32,33] To determine whether this increased cytokine expression is sufficient to induce monocyte chemoattraction, a transwell migration assay was used to evaluate THP-1 human monocyte migration towards CMT1A and control SCP conditioned medium (Fig. 4b). In all three congruent models, significantly greater numbers of THP-1 monocytes migrated towards CMT1A SCP conditioned medium than controls, and this recruitment is disrupted by inhibition of MCP1 signaling through a neutralizing antibody (Fig. 4c).

PMP22 dose dependency as a pathologic mechanism in CMT1A.

Even though increased expression of PMP22 protein is accountable for CMT1A pathogenesis, there are a number of other genes in the duplicated chromosomal region whose involvement has not yet been investigated. Since *HS3ST3B1* which is neighboring gene of *PMP22* in the duplicated region emerged from the microarray analysis (Fig. 2e) in CMT1A-hiPSC-SCPs, we explored expression patterns of *PMP22* and *HS3ST3B1* in all three congruent Schwann cell models. Intriguingly, the CMT1A-SCPs achieved by the differentiation-based methodology showed significantly increased levels of both *PMP22* and *HS3ST3B1* whereas direct reprogramming-based hiNC-SCs did not show unified statistical significance in *HS3ST3B1* expression (Supplementary Fig. 10a-f). We next confirmed that increased inflammatory cytokines were indeed stimulated only by PMP22, and not HS3ST3B1, when it was exogenously expressed in healthy Schwann cells (Supplementary Fig. 10g). Notably, exogenous PMP22 expression in results in increased inflammatory cytokine expression in differentiated Schwann cells, but not in peripheral neurons (Supplementary Fig. 10h) derived from the same individuals. To determine the effect of PMP22 on the recruitment of monocytes, we utilized a CMT1A hiPSC line (CS67iCMT-n4)

and its TALEN-generated isogenic control hiPSC line (CS67iCMT-n4.ISO-control) to generate CMT1A and control hiPSC-Schwann cell precursors that only differ in *PMP22* gene dosage (Fig. 5a-d). Decreased *PMP22* gene dosage resulted in less *MCP1* and *CXCL1* gene expression (Fig. 5e-g), while dramatically reducing THP1-monocyte chemotaxis, suggesting a possible causal link between PMP22 and monocyte recruitment (Fig. 5h and Supplementary Fig. 10i).

This increased expression of CXCL1 and MCP1 protein from our CMT1A models was further verified in clinical patient samples. Sural nerve biopsies were obtained from two genetically diagnosed CMT1A patients and show significantly enriched levels of CXCL1 and MCP1 protein over control samples (Fig. 5i-j). Further immunohistochemistry staining showed recruitment of CD68+ monocytes/macrophages into a third CMT1A patient's intercostal nerve (Fig. 5k). Importantly, this patient is relatively young (28 year old female) and fairly early into her disease course (diagnosed with the CMT1A genetic duplication less than one year prior to biopsy), suggesting that CD68+ monocyte/macrophage recruitment may be part of her primary pathology rather than a secondary reaction to abnormal myelin. Whether CXCL-1 and MCP1 upregulation is directly responsible for the migration of monocytes/macrophages into the peripheral nerves of CMT1A patients requires further investigation. Similarly, future studies are needed to more precisely delineate the role of immunopathology in CMT1A pathogenesis.

Discussion

Human pluripotent stem cells and direct-lineage-conversion technology represent a powerful approach to probe disease pathophysiology in a patient-specific manner. Our study describes an efficient strategy to model a human genetic disease by employing cell-fate plasticity. In agreement with data from model organisms[32,33] and patient biopsies (Fig. 5i-k), we find that three congruent human models of CMT1A-Schwann cells reveal the up-regulation of CXCL1 and MCP-1 proteins, as well an associated infiltration of immune cells into nerve tissues.

Our defined protocol for the directed differentiation and prospective isolation of Schwann-cell precursors from hPSCs (human pluripotent stem cells; hiPSCs or hESCs) features a chemical compound-based activation/inhibition of developmentally relevant pathways to enable Schwann-cell fate specification in a relatively fast (21–23 days) and efficient (13.62% +/− 1.89 in hESCs, 13.56% +/− 0.8817 in control hiPSCs) manner. The FACS-purified cells can also be subsequently re-plated, allowing for the study of Schwann-cell intrinsic properties as well as the potential for *in vitro* maturation along the Schwann-cell lineage via extended culture times. Primary human Schwann cells are known for their low myelination efficiency in experimental settings[34], particularly compared to rodent Schwann cells and human oligodendrocytes. Considering that our CD49d+ cells robustly express *GPR126*[35], a gene critical for initiation of myelination, continued myelination studies should yield positive outcomes under *in vitro* and *in vivo* settings. The three healthy human Schwann-cell models profiled here still have distinct genetic signatures, reflecting their disparate epigenetic origins. This is reflected in their gene-ontology-analysis results, through early developmental characteristics in the hESC-derived Schwann-cell model, features of glial and

neuronal commitment in the hiPSC-derived Schwann-cell model, and markers of aging such as substantial immune and inflammatory gene expression in the hiNC-derived Schwann-cell model (Supplementary table 3). Intriguingly, most of the queried genes associated with aging were upregulated in the hiNC-derived Schwann-cell model compared to other models, comparable to previous studies about improved cellular maturity in direct converted models (Supplementary Fig. 6a)[36]. Given that dysmyelination involves impaired myelination by developmentally immature Schwann cells, and that it has been demonstrated to play an important role in several CMT1A rodent models[5,37], our hPSC-derived Schwann-cell precursors may be more useful for studying the dysmyelination seen in CMT1A, as these cells are in early developmental stages. In contrast, our hiNC-derived Schwann cells are likely a better model for studying impaired neuronal-Schwann cell signaling in CMT1A, as transcriptome analysis reveals enriched responsiveness to extracellular stimuli and robust cell-death-pathway expression, which may be related to inflammation and Schwann-cell death in clinical CMT1A patients. Although further studies will be needed to establish a robust and reproducible *in vitro* myelination by human Schwann cells, our CMT1A Schwann cells should comprise a reliable model for investigating the various CMT1A pathophysiological mechanisms in effect through both early and late developmental stages.

CMT1A is not clinically considered to be an inflammatory disorder, although there is some laboratory evidence to support this idea [32,33,38,39]. Our data might suggest that neutrophils or monocytes could be recruited to nerves of CMT1A patients, potentially in a CXCL1 and MCP-1 mediated manner. This idea could be corroborated by rodent studies, which have found that CMT1A mouse models overexpressing or mutating *PMP22* have increased macrophage infiltration in peripheral nerves[37–39], and that this is largely mediated by MCP-1[32]. By taking advantage of the plasticity of cellular identity through different reprogramming approaches, our results present an alternative method by which future hiPSC-based studies may also be validated through the use of congruent model systems.

Methods

SOX10 and OCT4 reporter line generation

The human embryonic stem cell line, H9 (also known as WA09) was modified to express eGFP under the SOX10 promoter, using the CRISPR/Cas9 genome editing system. Similarly, the H9 line was also modified to express eGFP under OCT4 promoter.

Schwann cell differentiation from hiPSCs and PGD-hESCs

Human pluripotent stem cells were plated and differentiated into putative SCPs. Briefly, colonies of pluripotent cells were rendered into single cells and plated on Geltrex, an artificial basement membrane-like matrix, in accordance with previous protocols[40]. They were then treated with a combination of small molecules to induce neuronal and Schwann cell differentiation. On day 0, to initiate differentiation, aspirate the medium and add KSR medium containing 10 μM SB-431542 and 500 nM LDN-193189. On day 2 change medium to KSR medium containing 10 μM SB-431542, 500 nM LDN-193189, 3 μM CHIR 99021, 10 μM DAPT. On day 4 change medium to KSR/NB (3:1) medium containing 3 μM CHIR 99021 and 10 μM DAPT (final concentrations are for the combined KSR/NB mixture). On

day 6, change medium to KSR/NB (1:1) medium containing 3 μM CHIR 99021 and 10 μM DAPT. On day 8, change medium to KSR/NB (1:3) medium containing 3 μM CHIR 99021 and 10 μM DAPT. On day 10, 14, and 18 change medium to NB medium containing 200 μM dibutyrl cAMP and 200 μM sodium L-ascorbate. Cell were maintained in this manner until day 21–23 of differentiation, when the cells are ready for purification. To assess for myelination, the differentiation cell culture with the Geltrex was maintained with the culture in NB medium with 200 μM sodium L-ascorbate for 4–5 months.

Schwann cell purification and culture from hiPSCs and PGD-hESCs

Briefly, SCPs were purified with Fluorescence Activated Cell Sorting (FACS) after 21–23 days of differentiation using a PE-conjugated antibody to the alpha4 integrin, CD49d (R&D Systems, FAB1354P).[41] After FACS, SCPs were replated onto tissue culture plates treated with fibronectin (R&D Systems, 1918-FN-02M) and laminin (Cultrex, R&D Systems, 3400–010-1) coated plates. (Plates were coated with 1ug/mL laminin and 2ug/mL fibronectin in PBS for 24 hours). Cells were maintained in culture for up to 80 days post-FACS using Neurobasal medium (Life Technologies, 21103–049) supplemented with L-glutamine (Life Technologies, 25030–081), B-27 supplement (Life Technologies, 12587–070), N2 supplement (Life Technologies, cat. no. 17502–048), and 1% fetal bovine serum (FBS) (Hyclone, cat. no. SH30070.03).

Purification of OCT4+ embryonic stem cell and SOX10+ Neural crest

H9 OCT4::eGFP cells were maintained clonally and OCT4:eGFP positive pluripotent cells were FACS purified. H9 SOX10::eGFP cells were plated and as described above for Schwann cell differentiation. For differentiation towards neural crest, on day 0, aspirate the medium and add KSR medium containing 10 μM SB-431542 and 500 nM LDN-193189. On day 2, change medium to KSR medium containing 10 μM SB-431542, 500 nM LDN-193189, 3 μM CHIR 99021. On day 3, change medium to KSR medium containing 10 μM SB-431542, 3 μM CHIR 99021. On day 4, change medium to KSR/NB (3:1) medium containing 3 μM CHIR 99021 (final concentrations are for the combined KSR/NB mixture). On day 7 of differentiation, SOX10::eGFP neural crest were FACS purified.

Immunofluorescence

Cells were fixed in 4% Paraformaldehyde for 20 minutes, then blocked and permeablized in 0.5%BSA and 0.1% Triton X-100 in PBS for 30 minutes. Primary antibodies were diluted 1:100 to 1:500 in 0.5%BSA and 0.1% Triton X-100 in PBS and samples were incubated overnight at 4 degrees. Secondary antibodies were diluted 1:1000 in 0.5%BSA and 0.1% Triton X-100 in PBS, and incubated 2 hours at room temperature. Primary antibodies can be found in Supplementary Information. Appropriate 488, 568, and 647-conjugated Alexa fluor secondary antibodies were utilized.

RNA extraction and real time PCR

Cells were homogenized in Trizol Reagent (Life Technologies, 15596–026) and manufacturer's protocols were followed to extract total RNA. Total RNA (0.5 ug) was reverse transcribed into cDNA using the High Capacity cDNA Reverse Transcription Kit

(Applied Biosystems, 4387406). Real time PCR was performed on an Eppendorf Realplex Mastercycler Ep gradient S. Cycling conditions are as follows: 95 degrees 2 min, 40 cycles (95 degrees 3 seconds, 60 degrees 30 seconds). Primer probes can be found in Appendix 1a. Data from real time PCR for microarray validation probes in hiPSCs, PGD-hESCs, and hiNC-SCs were displayed as fold change in CMT1A sample expression versus median gene expression in controls, and analyzed with the ratio paired t-test.

Microarray analysis (hESC vs neural crest vs Schwann cells)

For microarray analysis, total RNA from Oct4+ embryonic stem cells ($n = 3$), SOX10+ neural crest ($n = 3$), and CD49d+ SCPs ($n = 3$) were collected from three independent differentiations, were hybridized to the Affymetrix Primeview Human Gene Expression Array by the Johns Hopkins Deep Sequencing and Microarray Core, and analyzed in Partek. Transcripts that were up- and down-regulated 2-fold or greater with a p-value greater than 0.05 were further analyzed using DAVID and Ingenuity Pathway Analysis.

Microarray analysis (CMT1A hiPSCs vs controls hPSCs)

Four independently differentiated samples from CMT1A hiPSCs (three samples from one clone from patient 5148, one sample from one hiPSC clone from unrelated patient 5165) and controls (two samples from one clone from control patient 2623, two samples from hESC line H9) were submitted for microarray analysis. Samples were collected immediately after FACS purification, and were selected for a minimum of 1.5-fold *PMP22* gene upregulation by qRTPCR, to model the physiologically expected *PMP22* upregulation in CMT1A. Total RNA was extracted and hybridized to the Affymetrix Primeview Human Gene Expression Array by the Johns Hopkins Deep Sequencing and Microarray Core, and analyzed in Partek. All genes differentially expressed at least 3 standard deviations from the mean (corresponding to a fold change of 2.9x higher expression in CMT1A samples) were further analyzed in Ingenuity Pathway Analysis (IPA; Canonical Pathways function) and DAVID (Biological Process, Cellular Components, and Biocarta functions).

RNA sequencing

Total RNA from 21 samples of hiPSC-derived SCPs (CMT1A $n = 4$, control $n = 4$), hESC-derived SCPs (CMT1A $n = 4$, control $n = 2$), and hiNC-derived Schwann cell lineage cells (CMT1A $n = 3$, control $n = 4$) were analyzed by HiSeq Throughput Sequencing using TruSeq RNA Acccess Library Construction kit (Illumina). Two analyses were performed comparing gene transcripts across the three differentiation methodologies using control Schwann cell models in search of general difference between the three models, first with conventional methods and then with the ‘POWER KIT’. Conventional data analysis was performed by Macrogen (Cambridge, MA), and categorized by using Partek and DAVID for gene ontology analysis. To analyze using ‘POWER KIT’, RNA-seq raw reads were mapped onto NCBI GRCh38 release 89 transcriptome using Tophat2[42] and read counts for each transcript were measured using HTSeq-count[43]. Two-step voom transformation[19,44] was used to identify differentially expressed genes between samples (p-value <0.05 and fold change <0.5 or >2.0); Gene Ontology enrichment of the differentially expressed genes was analyzed with DAVID. Two subsequent analyses were performed comparing CMT1A Schwann cell transcripts vs control Schwann cell transcripts within each differentiation

model to find disease-specific transcriptional changes. Data analysis was performed by Macrogen (Cambridge, MA), and categorized by using Partek, DAVID, and Ingenuity Pathway Analysis for pathologic gene ontology and pathway analysis. RNA sequencing data has been uploaded to GEO under accession code GSE85598.

Acute nerve crush transplantation model and histology

GFP+ CD49d+ SCPs were isolated from BC1, an hiPSC line constitutively expressing GFP (courtesy of Dr. Linzhao Cheng, Johns Hopkins University).

All animal procedures were carried out in accordance with and under protocols approved by the Johns Hopkins University IACUC. 4 months old male NOD.CB17-Prkdcscid/J mice (The Jackson Laboratory, 001303) were anesthetized under inhalation anesthesia of 1–3% isoflurane using VetEquip system. The left Tibial Nerve was exposed and a 5 mm segment just distal to the sciatic trifurcation underwent freeze/thaw twice with dry ice to kill all live cells (freeze with dry ice for 30 sec. and thaw 2 min.). The damage area was marked with two sutures on the surface of the tibial nerve, flanking the distal and proximal ends of the damage stump. Then the left tibial nerve was transected at 2mm above the proximal end of damage stump and secured using 10–0 sutures. Two microliters of GFP+ CD49d+ cells (40,000/per μl) were transplanted to the freeze/thaw damage stump.

Six weeks after GFP+ CD49d+ cell transplantation, animals were anesthetized and perfused with 4% paraformaldehyde. The previous surgical site was exposed; a portion of the tibial nerve (between 2 suture site) was harvested for immunohistochemistry and further fixed in 4% paraformaldehyde overnight. Paraformaldehyde-fixed nerves were cryoprotected by placing in a solution of 15% sucrose for 24 h followed by an additional 24 h in 30% sucrose. After embedding the tissue in OCT, serial 14-μm cross-sections were cut on a cryostat and stored at −20°C for later use. Sections were blocked in 0.2% Triton X-100 /PBS with 5% normal goat serum (NGS) for 1 h. They were subsequently incubated with the TUJ1 (BioLegend, 801202, 1:1000) antibody overnight at 4°C in 0.2% Triton X-100 /PBS containing 5% NGS. After the primary antibody incubation, the sections were washed thoroughly in 1xPBS, incubated with TEXAS RED-conjugated secondary antibody (1:200, Vector Laboratories) in PBS with 5% NGS for 45 min.

Chronic denervation transplantation model and catwalk gait analysis

All surgical procedures were performed on 6–8 week old Lewis rats. Anastomosis of freshly axotomized peroneal nerve to chronically denervated tibial nerve stump was performed as previously described.[3,4] Comparison groups included control hiPSC-Schwann cell precursor injection during anastomosis (n = 4 animals) vs PBS sham treatment (n = 3 animals). Treatment group received 80,000 control hiPSC-Schwann cell precursors (derived from patient 01582) in 6uL injections into the distal nerve stump (vs 6uL PBS sham treatment) using a 33-gauge needle attached to a custom made 10-μl syringe. After injecting the cells, the needle was kept in place for 2 min and withdrawn slowly. To prevent acute rejection episodes of transplanted hiPSC-Schwann cell precursors, 50 ug/mL of oral cyclosporine (Neoral, Novartis) was added to drinking water from 3 days before transplantation until the end of the study.

The CatWalk XT™ (Noldus Information Technology, Wageningen, Netherlands) assesses gait changes in rodents based on quantitative recordings of gait patterns as well as paw print characteristics. In order to evaluate functional outcomes while walking, footprints were captured and recorded by a camera located underneath the glass plate. Testing occurred 10 weeks after hiPSC-Schwann cell precursor transplantation. Each animal was recorded 4 times within the device; all runs were averaged and the results represent a single value. Recorded parameters include stand phase mean (average duration of contact of paws with glass plate), print width and length (width and length of paw print on glass plate, respectively), and maximum contact area (paw surface area in contact with glass at moment of maximum contact). Results were analyzed by examining the ratio of each parameter in the transplanted limb to the contralateral uninjured limb. All parameters had a pre-surgery ratio of one, signifying that both limbs were functioning equally prior to surgery.

CMT1A induced pluripotent stem cell generation

Fibroblasts from four CMT1A patients were obtained from the Coriell Biorepository (GM05146, GM05148, GM05165, GM05167). Fibroblasts were reprogrammed into induced pluripotent stem cells using previously reported methods[45] and the Cytotune Sendai Reprogramming Kit (LifeTech A1378001). After 2 weeks of reprogramming, IPS cells were identified by their colony morphology and replated onto mouse embryonic fibroblast (MEF) feeder layers. They were maintained on MEF feeder layers through weekly passaging for up to 50 passages. Lines were regularly assessed to be free of mycoplasma contamination. The 18 hiPSC clones initially generated were screened for expression of the genes *HHLA1* and *LincROR*, which were shown by Yamanaka's group to predict clones would be differentiation-defective versus differentiation competent[46], and *microRNA 371* cluster expression, which was shown to predict differentiation towards neuronal lineages.[47] Based on the results of our screens (data not shown), five of the 18 CMT1A-hiPSC clones were chosen for further studies. Due to variability in *PMP22* expression levels, matched pairs of CMT1A hiPSC-Schwann cell precursors and controls hiPSC-SCPs with at least a *PMP22* upregulation of 1.5x were used for subsequent experiments to best model CMT1A physiology.

Generation and genome editing of CMT1A-iPSCs

Line CS67iCMT-n4 was generated at the Cedars-Sinai iPSC core facility as previously[48], and is available at https://www.cedars-sinai.edu/Research/Research-Cores/Induced-Pluripotent-Stem-Cell-Core-/Stem-Cell-Lines.aspx (IRB protocol #Pro00031100) Confirmation of the PMP22 duplication was performed using multiplexed ligation dependent probe amplification (MLPA) analysis of the parental line. To generate the isogenic control line, a pair of TALENs was designed targeting the start codon region of PMP22 (Cellectis Bioresearch), and 2A-GFP and 2A-RFP were then cloned into the left and right TALENs respectively. Using the NEON Transfection System (Thermo fisher) TALENs were transfected into CS67iCMT. After transfection (48 hours), GFP and RFP double-positive cells were sorted and cultured for 7 to 10 days. Healthy iPSCs were dissociated into single cells using Accutase and plated at 10,000 cells per 10-cm dish. Rock inhibitor (Y-27632) was added at each passage. Upon forming colonies, individual clones were picked and plated into individual wells in a 96-well plate. After the colonies reached a size large

enough to cover half the area of a well, colonies were split into two plates via manual dissection. One plate was used to confirm the genotype via Sanger sequencing and MLPA. The other plate was either expanded or frozen until editing confirmation. Upon confirmation of editing of one of the three copies of PMP22, the lines were expanded and characterized by karyotyping.

Secreted protein expression profiling

Pairs of CMT1A SCPs and matched controls with at least 1.5 fold *PMP22* upregulation were identified. FACs purified CD49d+ SCPs from hiPSCs and PGD-hESCs were maintained in culture for 10 days post-FACS. For secreted protein profiling from hiNC-Schwann cells, medium was changed to NB+1% FBS for the last 3 days of culture. Cell conditioned medium was profiled with the Human Cytokine Array Kit (R&D Systems, ARY005).

Transwell migration assay

THP-1 human monocyte chemotaxis assays were performed by using the HTS transwell plate system (5μm pore size, Corning). Conditioned medium was collected from Day 10 post-FACS hiPSC- and PGD-hESC-SCPs, and 2–5 week post FACS hiNC-Schwann cells, and 100uL of Schwann cell conditioned medium was placed in bottom well with or without anti-MCP1 (R&D). THP-1 monocytes were resuspended in Neurobasal medium (Gibco) + 1% FBS to a concentration of 2.5 million cells/mL, and 100ul was placed in upper wells. After 3 hrs incubation in 37 ˚C with 5% CO2, migrated THP-1 cells were counted. n defined by independent assays.

CMT1A Preimplantation Genetic Diagnosis embryonic stem (PGD-hESC) cell line generation

Two embryonic stem cell lines with a preimplantation genetic diagnosis of CMT1A were obtained from the NIH Human Embryonic Stem Cell Repository (HUES PGD11 and 12; NIH registration numbers 94 and 95; NIH approval numbers NIHhESC-11–0094 and NIHhESC-11–0095). Embryonic stem cell lines were generated from blastocysts that were determined to have the CMT1A duplication through pre-implantation genetic diagnosis. The hESC line H9 (WA09) was used as a control. Lines were regularly assessed to be free of mycoplasma contamination. Matched pairs of CMT1A PGD-hESC-SCPs and H9-derived control SCPs with at least a *PMP22* upregulation of 1.5x were used for subsequent experiments.

CMT1A Induced Neural Crest-derived Schwann cell generation

Three CMT1A patient fibroblasts (from patients 5146, 5148, 5165) and two matching controls (from patients 0498 and 5756) were reprogrammed into induced neural crest and FACS purified using published methods[5]. hiNCs were maintained in Neurobasal medium containing 1 ug/ml of doxycycline for 3 days, followed by one more week of incubation with hiNC derived Schwann cell conditioned medium containing CNTF (10 ng/ml) and NRG1 (20 ng/ml), without doxycycline. Cells were maintained in culture for 2–5 weeks post-FACS.

CMT1A patient nerve biopsy procurement and analysis

To evaluate CXCL1 and MCP-1 protein expression, de-identified sural nerve biopsies from two patients with genetically proven CMT1A (two women, ages 26 and 50) and two histologically normal samples from non-CMT1A patients (two women, ages 55 and 79) were obtained from the Johns Hopkins Neuromuscular Histopathology Laboratory under appropriate Institutional Review Board (IRB) supervision with informed consent. Lysates were obtained by sonicating nerve biopsies in RIPA buffer, and equal amounts of protein were then used for secreted protein expression profiling (R&D Systems, ARY005).

To evaluate the presence of CD68+ monocytes/macrophages, a diagnostic biopsy of the intercostal nerve was done in a 28 year old female patient with genetically confirmed CMT1A to evaluate for enlargement of her nerves and to rule out Schwannomatosis (under same IRB as above). She was diagnosed with CMT1A only a year prior to biopsy when she presented with pain and enlarged nerve roots and lumbosacral and brachial plexi. The biopsy showed classic features of an inherited demyelinating neuropathy with axonal loss and many mature onion bulbs. CD-68 immunostaining was performed in paraffin embedded sections with anti-CD68 antibody (DAKO cat # M071801–5) using standard immunohistochemical methods (Vectastain kit).

Constructs and Electroporation

To validate the effect of *PMP22* or *HS3ST3B1*, each gene was amplified from cDNA library of H9 and inserted into the pcDNA3.1/V5-His plasmid by using TOPO TA system (Thermo Fisher Scientific, USA). To induce overexpression of these genes in hiPSC-derived Schwann cells or peripheral neurons, each cell population was prepared in 24 well plates with serum free medium including 10 ug of plasmid, and plasmid was transferred into cells by using the adherent cell electrode and NEPA21 (Nepa Gene, Japan).

Statistical analyses

Data was analyzed using Graphpad Prism 7. Means +/− standard deviation is plotted, and p-values were calculated using the unpaired t test, ratio paired t test, and one-way ANOVA as noted. A normal distribution was assumed. The n refers to cells from independent differentiations, unless otherwise specified.

Supplementary Material

Refer to Web version on PubMed Central for supplementary material.

Acknowledgements

The work in the Lee lab was supported by grants from the Robertson Investigator Award from New York Stem Cell Foundation (G.L.), the CMT Association (G.L.), the National Institutes of Health through the R01NS093213 (G.L.), the Muscular Dystrophy Association (G.L.) and the Maryland Stem Cell Research Fund (MSCRF/TEDCO) (G.L.). We also ackowledge salary support from the Johns Hopkins MD/PhD program (B.M-C.), the FARMS Fellowship (B.M-C.), the Adrienne Helis Malvin Medical Research Foundation (G.L., Y.O.) and the Global Research and Development Center (GRDC) Program through the National Research Foundation of Korea (NRF) funded by the Ministry of Education, Science and Technology (2017K1A4A3014959). The work in the Kim lab was supported by grants from Kyung Hee University in 2016 (KHU-20160535), the Korea Health Technology R&D Project through the Korea Health Industry Development Institute (KHIDI) funded by the Ministry of Health & Welfare, Republic of Korea (HI16C2216) and NRF grant funded by the Korea government

(NRF-2017R1C1B3009321, NRF-2017M3C7A1047640 and NRF-2017M3A9E4047243). The work in the Baloh lab was supported by grants RN3–06530 (California Institute for Regenerative Medicine) and NS097545 (National Institutes of Health). The work in the Studer lab was supported by the New York State Stem Cell Fund (G.L., K.E. and L.S.). The work in the Hoke lab was supported by the Maryland Stem Cell Research Fund (MSCRF/TEDCO) and the Dr. Miriam and Sheldon G. Adelson Medical Research Foundation. The work in the Brandacher lab was supported by the Maryland Stem Cell Research Fund (MSCRF/TEDCO).

References

1. Park IH et al. Disease-specific induced pluripotent stem cells. Cell 134, 877–886, doi:10.1016/j.cell.2008.07.041 (2008). [PubMed: 18691744]
2. Lee G et al. Modelling pathogenesis and treatment of familial dysautonomia using patient-specific iPSCs. Nature 461, 402–406, doi:10.1038/nature08320 (2009). [PubMed: 19693009]
3. Mertens J et al. Directly Reprogrammed Human Neurons Retain Aging-Associated Transcriptomic Signatures and Reveal Age-Related Nucleocytoplasmic Defects. Cell Stem Cell 17, 705–718, doi:10.1016/j.stem.2015.09.001 (2015). [PubMed: 26456686]
4. van Paassen BW et al. PMP22 related neuropathies: Charcot-Marie-Tooth disease type 1A and Hereditary Neuropathy with liability to Pressure Palsies. Orphanet J Rare Dis 9, 38, doi:10.1186/1750-1172-9-38 (2014). [PubMed: 24646194]
5. Robaglia-Schlupp A et al. PMP22 overexpression causes dysmyelination in mice. Brain 125, 2213–2221 (2002). [PubMed: 12244079]
6. Passage E et al. Ascorbic acid treatment corrects the phenotype of a mouse model of Charcot-Marie-Tooth disease. Nat Med 10, 396–401, doi:10.1038/nm1023 (2004). [PubMed: 15034573]
7. Burns J et al. Ascorbic acid for Charcot-Marie-Tooth disease type 1A in children: a randomised, double-blind, placebo-controlled, safety and efficacy trial. Lancet Neurol 8, 537–544, doi:10.1016/S1474-4422(09)70108-5 (2009). [PubMed: 19427269]
8. Verhamme C et al. Oral high dose ascorbic acid treatment for one year in young CMT1A patients: a randomised, double-blind, placebo-controlled phase II trial. BMC Med 7, 70, doi:10.1186/1741-7015-7-70 (2009). [PubMed: 19909499]
9. Pareyson D et al. Ascorbic acid in Charcot-Marie-Tooth disease type 1A (CMT-TRIAAL and CMT-TRAUK): a double-blind randomised trial. Lancet Neurol 10, 320–328, doi:10.1016/S1474-4422(11)70025-4 (2011). [PubMed: 21393063]
10. Micallef J et al. Effect of ascorbic acid in patients with Charcot-Marie-Tooth disease type 1A: a multicentre, randomised, double-blind, placebo-controlled trial. Lancet Neurol 8, 1103–1110, doi:10.1016/S1474-4422(09)70260-1 (2009). [PubMed: 19818690]
11. Lewis RA et al. High-dosage ascorbic acid treatment in Charcot-Marie-Tooth disease type 1A: results of a randomized, double-masked, controlled trial. JAMA Neurol 70, 981–987, doi:10.1001/jamaneurol.2013.3178 (2013). [PubMed: 23797954]
12. Suter U et al. Regulation of tissue-specific expression of alternative peripheral myelin protein-22 (PMP22) gene transcripts by two promoters. J Biol Chem 269, 25795–25808 (1994). [PubMed: 7929285]
13. Heine W, Conant K, Griffin JW & Hoke A Transplanted neural stem cells promote axonal regeneration through chronically denervated peripheral nerves. Exp Neurol 189, 231–240, doi:10.1016/j.expneurol.2004.06.014 (2004). [PubMed: 15380475]
14. Fu SY & Gordon T Contributing factors to poor functional recovery after delayed nerve repair: prolonged denervation. J Neurosci 15, 3886–3895 (1995). [PubMed: 7751953]
15. Katona I et al. PMP22 expression in dermal nerve myelin from patients with CMT1A. Brain 132, 1734–1740, doi:10.1093/brain/awp113 (2009). [PubMed: 19447823]
16. Akdis M et al. Interleukins, from 1 to 37, and interferon-gamma: receptors, functions, and roles in diseases. J Allergy Clin Immunol 127, 701–721 e701–770, doi:10.1016/j.jaci.2010.11.050 (2011). [PubMed: 21377040]
17. Turner MD, Nedjai B, Hurst T & Pennington DJ Cytokines and chemokines: At the crossroads of cell signalling and inflammatory disease. Biochim Biophys Acta 1843, 2563–2582, doi:10.1016/j.bbamcr.2014.05.014 (2014). [PubMed: 24892271]

18. Kim YJ et al. Generation of multipotent induced neural crest by direct reprogramming of human postnatal fibroblasts with a single transcription factor. Cell Stem Cell 15, 497–506, doi:10.1016/j.stem.2014.07.013 (2014). [PubMed: 25158936]
19. Germain PL & Testa G Taming Human Genetic Variability: Transcriptomic Meta-Analysis Guides the Experimental Design and Interpretation of iPSC-Based Disease Modeling. Stem Cell Reports 8, 1784–1796, doi:10.1016/j.stemcr.2017.05.012 (2017). [PubMed: 28591656]
20. Wu J et al. Insertional Mutagenesis Identifies a STAT3/Arid1b/beta-catenin Pathway Driving Neurofibroma Initiation. Cell Rep 14, 1979–1990, doi:10.1016/j.celrep.2016.01.074 (2016). [PubMed: 26904939]
21. Woodhoo A et al. Notch controls embryonic Schwann cell differentiation, postnatal myelination and adult plasticity. Nat Neurosci 12, 839–847, doi:10.1038/nn.2323 (2009). [PubMed: 19525946]
22. D'Antonio M et al. TGFbeta type II receptor signaling controls Schwann cell death and proliferation in developing nerves. J Neurosci 26, 8417–8427, doi:10.1523/JNEUROSCI.1578-06.2006 (2006). [PubMed: 16914667]
23. Clements MP et al. The Wound Microenvironment Reprograms Schwann Cells to Invasive Mesenchymal-like Cells to Drive Peripheral Nerve Regeneration. Neuron 96, 98–114 e117, doi:10.1016/j.neuron.2017.09.008 (2017). [PubMed: 28957681]
24. Lee SM, Chin LS & Li L Dysregulation of ErbB Receptor Trafficking and Signaling in Demyelinating Charcot-Marie-Tooth Disease. Mol Neurobiol 54, 87–100, doi:10.1007/s12035-015-9668-2 (2017). [PubMed: 26732592]
25. Nickols JC, Valentine W, Kanwal S & Carter BD Activation of the transcription factor NF-kappaB in Schwann cells is required for peripheral myelin formation. Nat Neurosci 6, 161–167, doi:10.1038/nn995 (2003). [PubMed: 12514737]
26. Tang W et al. Expression of Nrf2 Promotes Schwann Cell-Mediated Sciatic Nerve Recovery in Diabetic Peripheral Neuropathy. Cell Physiol Biochem 46, 1879–1894, doi:10.1159/000489373 (2018). [PubMed: 29719281]
27. Mey J, Schrage K, Wessels I & Vollpracht-Crijns I Effects of inflammatory cytokines IL-1beta, IL-6, and TNFalpha on the intracellular localization of retinoid receptors in Schwann cells. Glia 55, 152–164, doi:10.1002/glia.20444 (2007). [PubMed: 17078027]
28. Zhang G et al. Hypothalamic programming of systemic ageing involving IKK-beta, NF-kappaB and GnRH. Nature 497, 211–216, doi:10.1038/nature12143 (2013). [PubMed: 23636330]
29. Trujillo G et al. Neutrophil recruitment to the lung in both C5a- and CXCL1-induced alveolitis is impaired in vitamin D-binding protein-deficient mice. J Immunol 191, 848–856, doi:10.4049/jimmunol.1202941 (2013). [PubMed: 23752613]
30. Vries MH et al. CXCL1 promotes arteriogenesis through enhanced monocyte recruitment into the peri-collateral space. Angiogenesis 18, 163–171, doi:10.1007/s10456-014-9454-1 (2015). [PubMed: 25490937]
31. Deshmane SL, Kremlev S, Amini S & Sawaya BE Monocyte chemoattractant protein-1 (MCP-1): an overview. J Interferon Cytokine Res 29, 313–326, doi:10.1089/jir.2008.0027 (2009). [PubMed: 19441883]
32. Kohl B, Fischer S, Groh J, Wessig C & Martini R MCP-1/CCL2 modifies axon properties in a PMP22-overexpressing mouse model for Charcot-Marie-tooth 1A neuropathy. Am J Pathol 176, 1390–1399, doi:10.2353/ajpath.2010.090694 (2010). [PubMed: 20093502]
33. Kobsar I, Hasenpusch-Theil K, Wessig C, Muller HW & Martini R Evidence for macrophage-mediated myelin disruption in an animal model for Charcot-Marie-Tooth neuropathy type 1A. J Neurosci Res 81, 857–864, doi:10.1002/jnr.20601 (2005). [PubMed: 16041800]
34. Lehmann HC et al. Human Schwann cells retain essential phenotype characteristics after immortalization. Stem Cells Dev 21, 423–431, doi:10.1089/scd.2010.0513 (2012). [PubMed: 21585251]
35. Monk KR et al. A G protein-coupled receptor is essential for Schwann cells to initiate myelination. Science 325, 1402–1405, doi:10.1126/science.1173474 (2009). [PubMed: 19745155]
36. Wainger BJ et al. Modeling pain in vitro using nociceptor neurons reprogrammed from fibroblasts. Nat Neurosci 18, 17–24, doi:10.1038/nn.3886 (2015). [PubMed: 25420066]

37. Meyer Zu Horste G & Nave KA Animal models of inherited neuropathies. Curr Opin Neurol 19, 464–473, doi:10.1097/01.wco.0000245369.44199.27 (2006). [PubMed: 16969156]
38. Chittoor VG et al. Biochemical characterization of protein quality control mechanisms during disease progression in the C22 mouse model of CMT1A. ASN Neuro 5, e00128, doi:10.1042/AN20130024 (2013). [PubMed: 24175617]
39. Misko A, Ferguson T & Notterpek L Matrix metalloproteinase mediated degradation of basement membrane proteins in Trembler J neuropathy nerves. J Neurochem 83, 885–894 (2002). [PubMed: 12421361]
40. Chambers SM et al. Combined small-molecule inhibition accelerates developmental timing and converts human pluripotent stem cells into nociceptors. Nat Biotechnol 30, 715–720, doi:10.1038/nbt.2249 (2012). [PubMed: 22750882]
41. Jessen KR & Mirsky R The origin and development of glial cells in peripheral nerves. Nat Rev Neurosci 6, 671–682, doi:10.1038/nrn1746 (2005). [PubMed: 16136171]
42. Kim D et al. TopHat2: accurate alignment of transcriptomes in the presence of insertions, deletions and gene fusions. Genome Biol 14, doi:ARTN R36 10.1186/gb-2013-14-4-r36 (2013).
43. Anders S, Pyl PT & Huber W HTSeq-a Python framework to work with high-throughput sequencing data. Bioinformatics 31, 166–169, doi:10.1093/bioinformatics/btu638 (2015). [PubMed: 25260700]
44. Ritchie ME et al. limma powers differential expression analyses for RNA-sequencing and microarray studies. Nucleic Acids Res 43, doi:ARTN e47 10.1093/nar/gkv007 (2015).
45. Choi IY, Lim H & Lee G Efficient generation human induced pluripotent stem cells from human somatic cells with Sendai-virus. J Vis Exp, doi:10.3791/51406 (2014).
46. Koyanagi-Aoi M et al. Differentiation-defective phenotypes revealed by large-scale analyses of human pluripotent stem cells. Proc Natl Acad Sci U S A 110, 20569–20574, doi:10.1073/pnas.1319061110 (2013). [PubMed: 24259714]
47. Kim H et al. miR-371–3 expression predicts neural differentiation propensity in human pluripotent stem cells. Cell Stem Cell 8, 695–706, doi:10.1016/j.stem.2011.04.002 (2011). [PubMed: 21624813]
48. Sareen D et al. Targeting RNA foci in iPSC-derived motor neurons from ALS patients with a C9ORF72 repeat expansion. Sci Transl Med 5, 208ra149, doi:10.1126/scitranslmed.3007529 (2013).

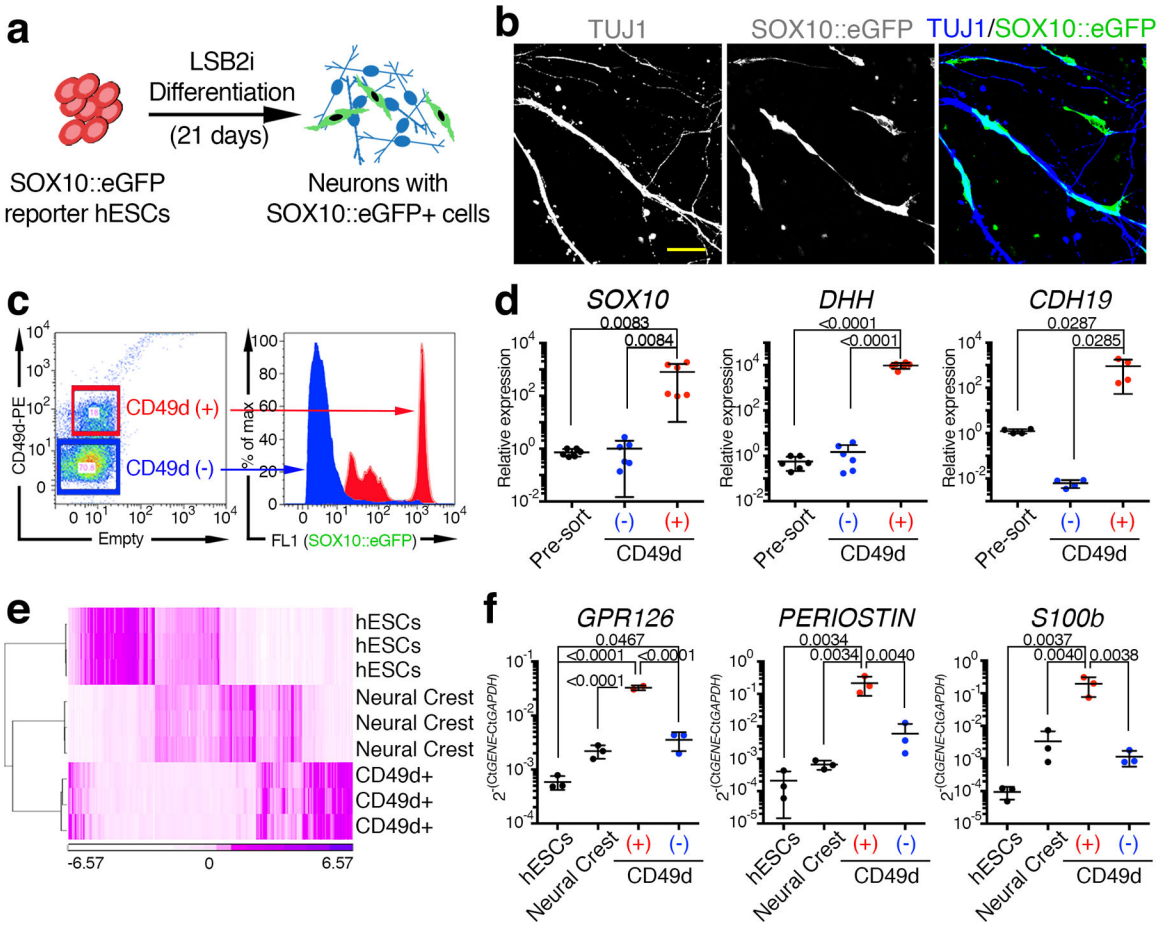

Fig. 1 |. Directed differentiation and prospective isolation of Schwann cells from human embryonic stem cells.

a, Schematic of LSB2i differentiation using H9 SOX10::eGFP reporter hESCs. **b**, Immunofluorescence for eGFP and TUJ1 demonstrate SOX10+ SCPs in association with TUJ1+ neurons (bar = 50 μm). **c**, Flow cytometry demonstrates substantial overlap between the CD49d+ population and SOX10::eGFP expression. **d**, Real time PCR for Schwann cell lineage markers in CD49d+ putative SCPs, CD49d- non- SCPs, and unsorted cells. Data expressed as mean +/− SD (n = 6, independent samples) and p-values calculated by one-way ANOVA. **e**, Heat map representation of supervised hierarchical clustering of OCT4::eGFP+ hESCs, SOX10::eGFP+ neural crest, and CD49d+ putative SCPs, based on all differentially expressed genes with $p<0.001$. **f**, Validation of microarray results with qRT-PCR for select SCP genes, normalized to *GAPDH*. Data expressed as mean +/− SD (n = 3, independent samples) and p-values calculated by one-way ANOVA.

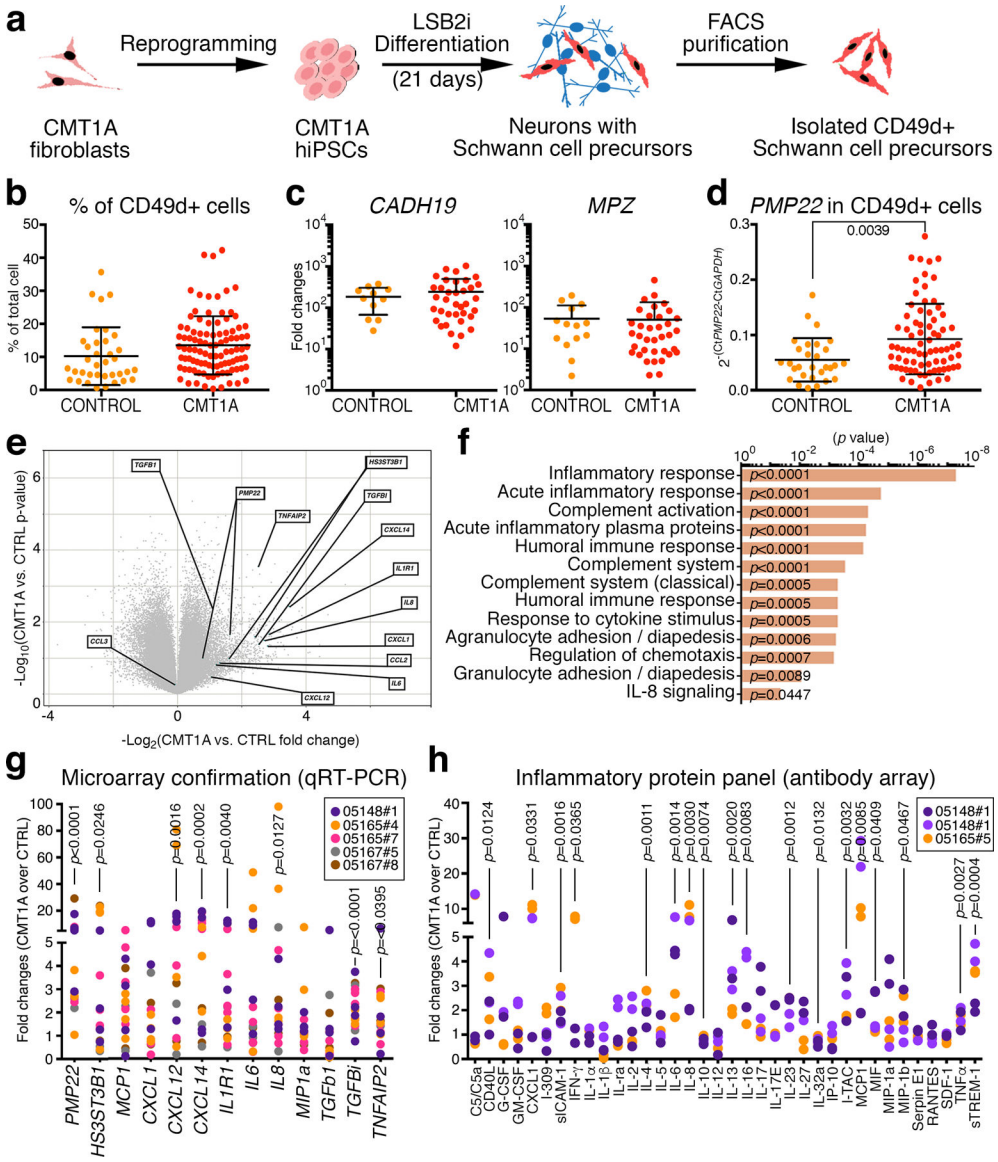

Fig. 2 |. Modelling CMT1A with human Schwann cells from patient-derived hiPSCs.

a, Schematic of the reprogramming methods to generate CMT1A patient hiPSC derived SCPs from CMT1A patient fibroblasts. **b**, FACS purification of LSB2i treated CMT1A and control hiPSCs reveals similar yields of CD49d+ SCPs. Data expressed as mean +/− SD (control $n = 36$, CMT1A $n = 9$, independent samples) and p-values calculated by unpaired t-test. **c**, Post-FACS evaluation of Schwann cell lineage gene enrichment in CD49d+ hiPSC-SCPs versus matched CD49d- non-SCPs, by real time PCR. Data expressed as mean +/− SD (control $n = 11$ for *CDH19* and n = 15 for *MPZ*, CMT1A $n = 28$ for *CDH19* and $n = 37$ for *MPZ*, independent samples) and p-values calculated by unpaired t-test. **d**, Real time PCR for *PMP22* in CMT1A and control CD49d+ hiPSC-SCPs. Data expressed as mean +/− SD (control $n = 29$, CMT1A $n = 76$, independent samples) and p-values calculated by unpaired t-test. **b-d**, Analysis includes five control hPSC lines representing four genotypes and seven CMT1A hiPSC lines representing four genotypes. **e**, Volcano plot representation of

microarray array expression profiling of four biologically independent CMT1A SCP samples and four biologically independent control hPSC-SCP samples. Select genes of interest highlighted and designated for validation with qRT-PCR. **f**, Results from DAVID gene ontology and Ingenuity Pathway Analysis of differentially expressed genes. Data expressed as *p*-value of each pathway. **g**, Real time PCR validation of microarray results in biologically independent samples from five hiPSC clones representing three CMT1A patients. Data expressed as ratio of gene expression in CMT1A versus control hiPSC-derived SCPs. Data from independent clones are displayed as different colors, dots of same color are independent assays from same clone. Data expressed as ratio of gene expression in CMT1A SCPs versus matched control (05148#1 $n = 4$, 05148#4 $n = 4$, 05165#7 $n = 5$, 05167#5 $n = 2$, 05167#8 $n = 2$, independent samples) and *p*-values calculated by ratio paired t-test. **h**, Cytokine array profiling of cell conditioned medium from Day 10 post-FACS CMT1A and control SCPs. Data expressed as ratio of protein expression in CMT1A SCPs versus matched control (05148#1 $n = 4$, 05165#5 $n = 2$, independent samples) and *p*-values calculated by ratio paired t-test. Data from independent differentiations are displayed as different colors, dots of same color are from same differentiation.

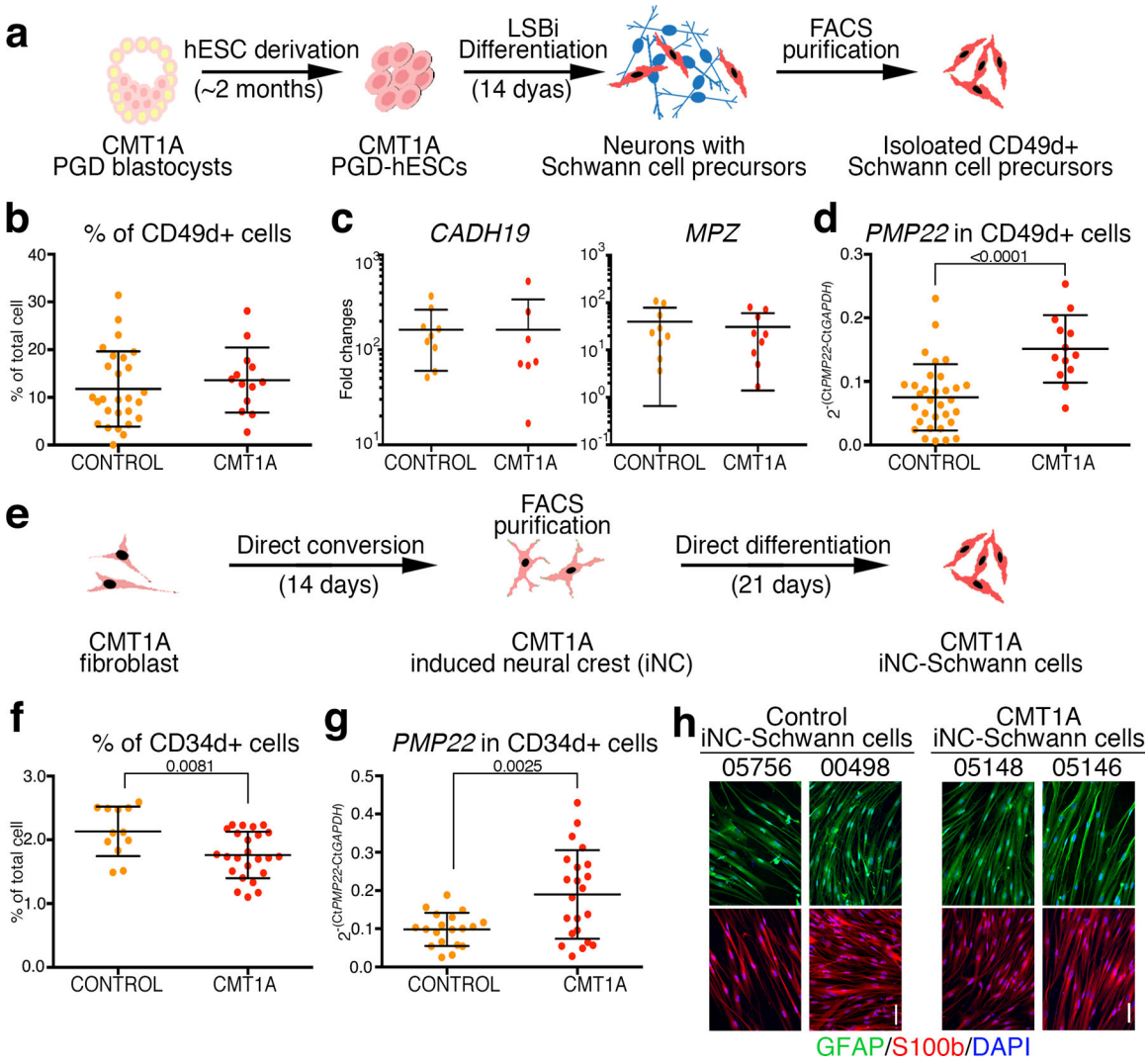

Fig. 3 |. Achievement of congruent CMT1A disease models by employing different cell fate manipulating methods.

a, Schematic of the method to generate CMT1A PGD-hESC derived SCPs from CMT1A blastocysts. **b**, FACS purification of LSB2i treated CMT1A and control PGD-hESCs reveals similar yields of CD49d+ PGD-hESC- SCPs. Data expressed as mean +/−SD (control n = 27, CMT1A n = 13, independent samples) and p-values calculated by unpaired t-test. **c**, Post-FACS evaluation of Schwann cell lineage gene enrichment in CD49d+ SCPs versus matched CD49d- non-SCPs, by real time PCR. Data expressed as mean +/−SD (control n = 9 for *CDH19* and n = 9 for *MPZ*, CMT1A n = 7 for *CDH19* and n = 9 for *MPZ*, independent samples) and p-values calculated by unpaired t-test. **d**, Real time PCR for *PMP22* in CMT1A and control CD49d+ SCPs. Data expressed as mean +/− SD (control n = 32, CMT1A n = 25, independent samples) and p-values calculated by unpaired t-test. **b-d**, Analysis includes two control hESC lines representing one genotype and two CMT1A PGD-hESC lines representing two genotypes. **e**, Schematic of the method to directly convert CMT1A patient fibroblasts into CMT1A hiNC-Schwann cells. **f**, FACS purification of CMT1A and control hiNCs by using CD34 antibody. Data expressed as mean +/−SD

(control $n = 12$, CMT1A $n = 24$, independent samples) and p-values calculated by unpaired t-test. **g**, Real time PCR for *PMP22* in CMT1A and control CD34+ Schwann cells. Data expressed as mean +/− SD (control $n = 19$, CMT1A $n = 22$, independent samples) and p-values calculated by unpaired t-test. **f-g**. Analysis includes two control fibroblast lines representing two control patients and three CMT1A fibroblast lines representing three CMT1A patients. **h**, Representative immunofluorescence for GFAP and S100b in hiNC-Schwann cells from two control fibroblasts and two CMT1A fibroblasts. (bar = 50 μm).

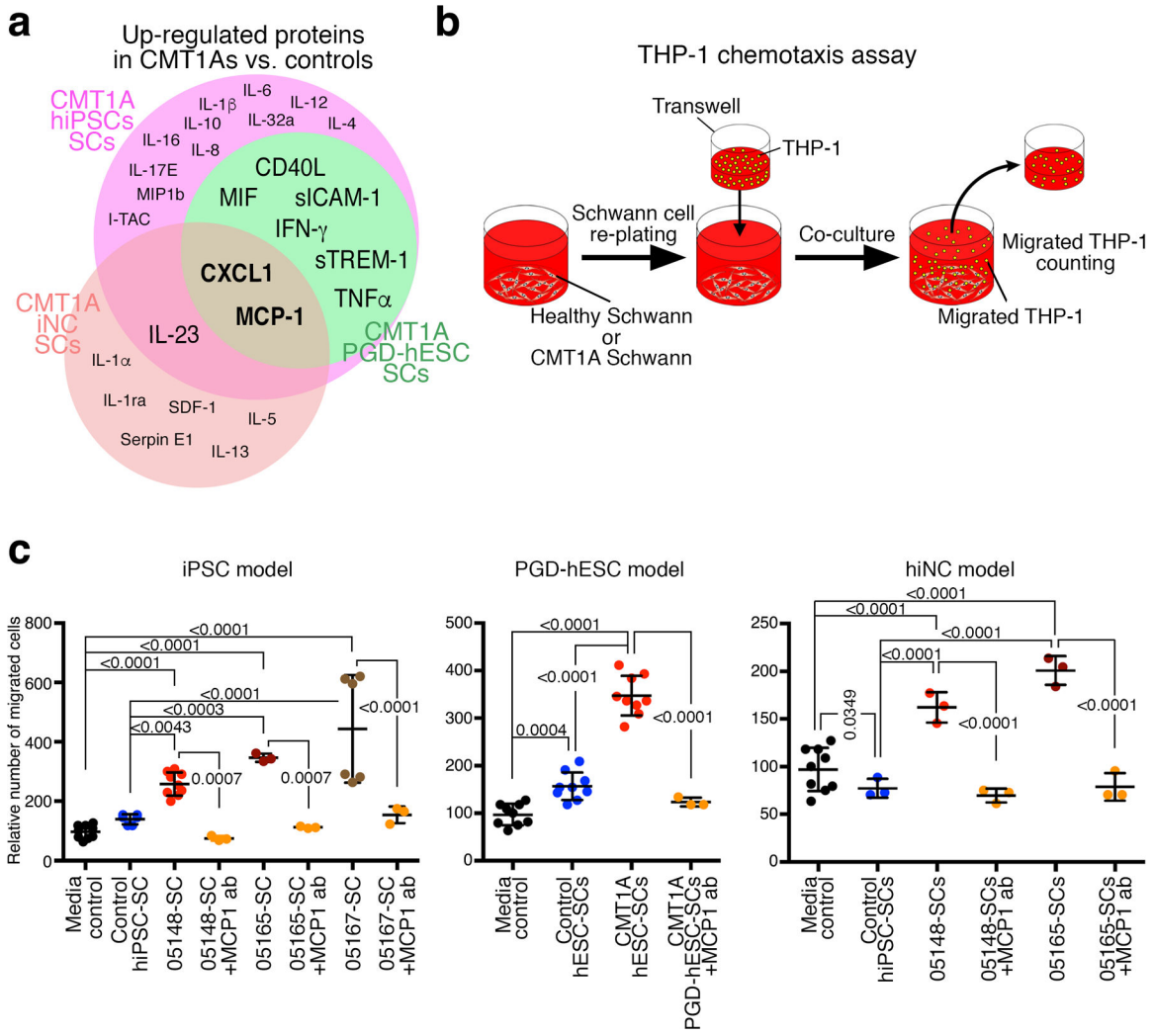

Fig. 4 |. Validation of the converged CMT1A phenotype from congruent Schwann cell models.

a, Venn diagram of upregulated secreted proteins in CMT1A hiPSC-, CMT1A PGD-hESC-, and CMT1A hiNC-derived Schwann cell models, with a converged phenotype of CXCL1 and MCP-1 protein upregulation. **b**, Illustration of how THP-1 monocyte recruitment is assessed in co-culture with Schwann cells. **c**, THP-1 human monocyte transwell migration assay results, using conditioned media of SCPs derived from CMT1A and control hiPSC lines for each model. Data expressed as mean +/− SD of migrated THP-1 cells (hiPSC-SCP control $n = 6$ and CMT1A $n = 6$ for each line, hESC-SCP control $n = 9$ and CMT1A $n = 9$ for each line, hiNC-SC control $n = 9$ and CMT1A $n = 3$ for each line, independent samples and independent assays) and p-values calculated by one-way ANOVA.

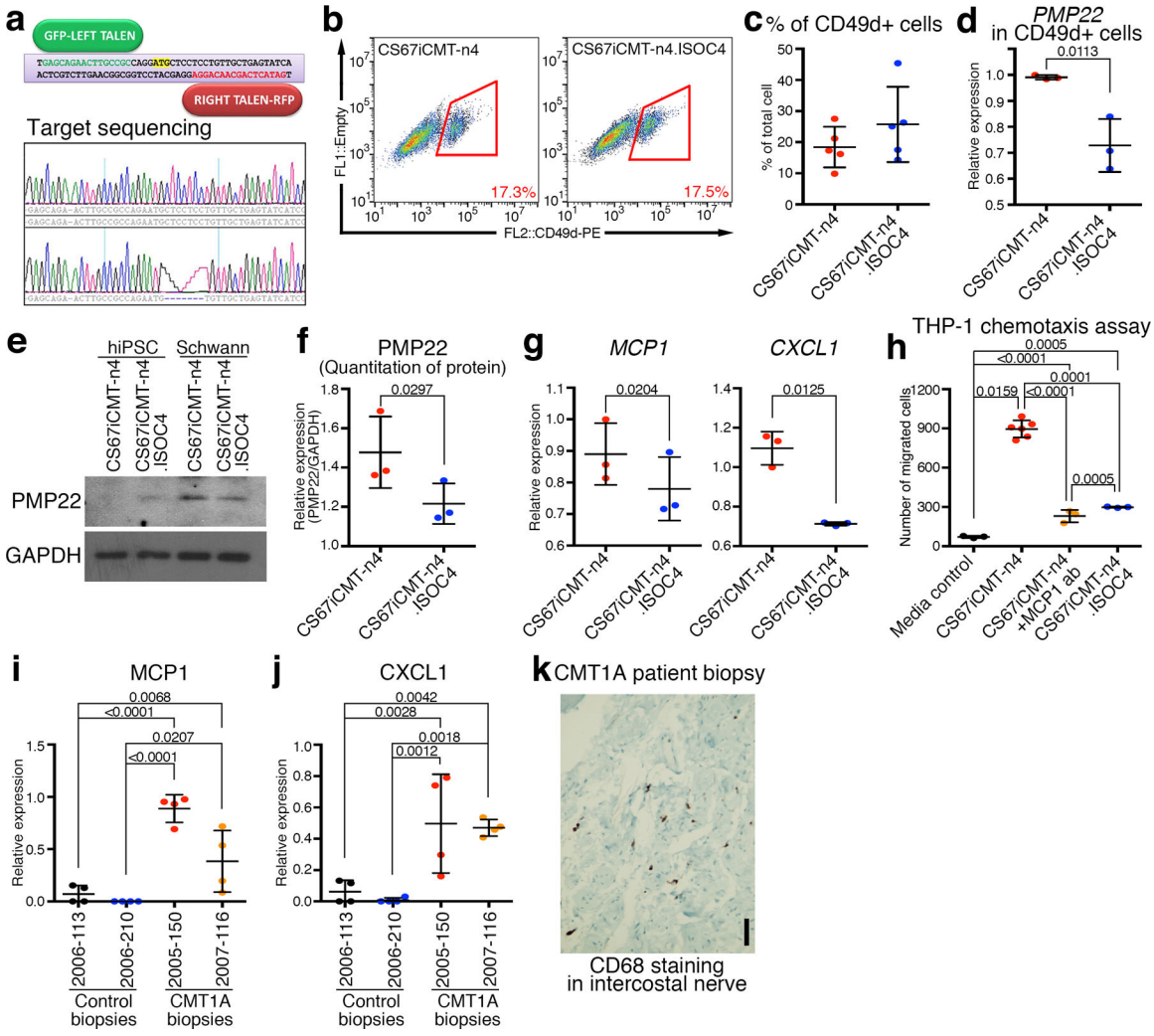

Fig. 5 |. Association between PMP22 gene dosage and inflammatory signatures.

a, TALEN-based gene editing results. Targeting sequences of TALEN-based exon editing for PMP22 (upper). Sequencing result of TALEN-based 2nd exon inactivation indicated target sequences harboring start codon were eliminated (lower). Efficiency of TALEN-based exon targeting with no off-target mutations in 16 predicted regions (47% clones with modifications and 12% clones with two copies of wild type and one copy of knock out alleles). **b**, Representative FACS plots from purification of CD49d+ Schwann cell precursors from CMT1A hiPSC (CS67iCMT-n4) and its isogenic control hiPSC (CS67iCMT-n4.ISOC4). **c**, Efficiency of differentiation from both lines. Data expressed as mean +/−SD (CMT1A $n = 5$, isogenic control $n = 5$, independent samples) and p-values calculated by paired t-test. **d**, Relative level of mRNA transcription of *PMP22* in CMT1A- and isogenic control Schwann cell precursors. Data expressed as mean +/−SD (CMT1A $n = 3$, isogenic control $n = 3$, independent samples) and p-values calculated by unpaired t-test. **e-f**, Protein expression level of PMP22 in undifferentiated hiPSCs and hiPSC-Schwann cells from the CMT1A hiPSC line and its isogenic control (**e** and Supplementary figure 11), and validation of protein band intensity (**f**). GAPDH was used as an internal control. Data expressed as mean +/−SD (CMT1A $n = 3$, isogenic control $n = 3$, independent samples) and p-values

calculated by paired t-test. **g**, Transcription level of *MCP1* and *CXCL1* in CMT1A hiPSC-derived- and isogenic control Schwann cells were validated by quantitative PCR. Data expressed as mean +/−SD (CMT1A $n = 3$, isogenic control $n = 3$, independent samples) and p-values calculated by paired t-test. **h**, Chemotaxis assay with THP1 monocytes was performed with media control, CMT1A-Schwann cells, CMT1A-Schwann cells with antibody neutralization, and isogenic control Schwann cells. Representative image of monocytes migrated into the Schwann cell side of the chamber. Data expressed as mean +/−SD (CMT1A $n = 6$, isogenic control $n = 3$, independent samples) and p-values calculated by one-way ANOVA. **i**, Protein expression level of CXCL1 in CMT1A and control patient nerve biopsies. Data expressed as mean +/− SD of cytokine dot array intensity ($n = 4$ for each sample, independent biopsies) and p-values calculated by one-way ANOVA. **j**, Protein expression level of MCP1 in CMT1A and control patient nerve biopsies. Data expressed as mean +/− SD of cytokine dot array intensity ($n = 4$ for each sample, independent biopsies) and p-values calculated by one-way ANOVA. **k**, CD68 staining (a marker for monocytes/macrophages, and immune-labelled cells appear as brown stained.) in intercostal nerve biopsy from a CMT1A patient (scale bar = 100 μm).

Table 1 |

Gene ontology and pathway analysis with upregulated gene list (CD49d positive cells over hESCs)

GO terms	p-value
Erbb signalling (Ingenuity IPA)	7.58578E-05
Neuregulin signalling (Ingenuity IPA)	0.000436
Gliogenesis (DAVID)	0.000430
PDGF signalling (Ingenuity IPA)	0.0120
CNTF signalling (Ingenuity IPA)	0.0135
Erbb signalling pathway (DAVID)	0.0370